NASA Technical Memorandum 82841

Laser Anemometer Using a Fabry-Perot Interferometer for Measuring Mean Velocity and Turbulence Intensity Along the Optical Axis in Turbomachinery

Richard G. Seasholtz and Louis J. Goldman
Lewis Research Center
Cleveland, Ohio

Prepared for the
Winter Annual Meeting of the American Society of Mechanical Engineers
Phoenix, Arizona, November 14–19, 1982

NASA

LASER ANEMOMETER USING A FABRY-PEROT INTERFEROMETER FOR MEASURING MEAN VELOCITY AND TURBULENCE INTENSITY ALONG THE OPTICAL AXIS IN TURBOMACHINERY

Richard G. Seasholtz and Louis J. Goldman

National Aeronautics and Space Administration
Lewis Research Center
Cleveland, Ohio

E-1211

ABSTRACT

A laser anemometer based on a confocal Fabry-Perot interferometer was developed to measure the mean velocity component along the optical axis. A technique for measuring a small optical-axis velocity component in a flow with a large transverse velocity component is presented. Experimental results are given for a subsonic free jet operating in a laboratory environment, and for a 0.508-meter diameter turbine stator cascade. Satisfactory operation of the instrument was demonstrated in the stator cascade facility with an ambient acoustic noise level during operation of about 105 dB. In addition, the turbulence intensity measured with the interferometer was consistent with previous measurements taken with a fringe-type laser anemometer.

INTRODUCTION

Laser anemometry has become an important diagnostic technique for studying flow fields in aircraft turbomachinery components with detailed flow studies having been made in both stator stages (1) and within rotor blade rows (2-4). However, the most commonly used laser anemometers (the dual-beam fringe system and the two-spot time-of-flight system) measure only velocity components normal to the optical axis. A requirement exists for measuring the velocity component along the optical axis as well as the transverse components. All three components of the flow field are needed to verify new three-dimensional computer codes and for secondary flow studies.

A number of constraints exist in designing a laser anemometer for turbomachinery studies. Among these are high flow velocities (typically up to Mach 1), limited optical access (usually f/4 or smaller), multiple surfaces close to the measurement region, and a need to minimize run time to reduce facility operating costs. In typical axial turbomachinery facilities optical access is limited to the radial direction and backscatter measurements are mandatory. Furthermore, the anemometer must reliably operate in the adverse environments found in test facilities - mechanical vibration, wide temperature ranges, and high acoustic noise levels.

Three basic approaches are applicable for measuring the velocity component along the optical axis. One approach is to use a fringe type system to measure three independent velocity components and then use these to calculate the optical-axis component. Fringe type systems have been developed that use color separation (5), polarization separation (6), and frequency separation (7,8) of the velocity components. This approach has the advantage of all fringe systems - the capability to effectively use scattered light collected over large apertures. Unfortunately, the error of the optical-axis component derived in this fashion becomes large when only velocity components close to the optical axis are measured (6,9).

A second approach to measure the optical-axis component is the reference beam or heterodyne technique. This approach has been used for long range atmospheric measurements (10) using CO_2 lasers and for measurements in a low velocity jet (11). In this method the scattered light is heterodyned with a local oscillator signal to obtain the Doppler shift frequency. For backscatter systems the Doppler shift is $2v/\lambda$ where v is the velocity component along the optical axis. For visible laser light the frequency shift is about 4 Mhz/meter/sec. This results in a large dynamic frequency range, which can easily exceed the frequency response of commonly used photomultiplier tubes for the large optical-axis velocity components that may occur in turbomachinery. A fundamental limitation of heterodyne systems is that the maximum effective receiver aperture area is limited by the Antenna Theorem (12) to about λ^2/Ω where Ω is the solid angle subtended by the probe volume at the receiver aperture.

The third approach, which is the subject of this paper, is the use of a high resolution interferometer to directly measure the Doppler shift. This technique has previously been used by other workers to measure the transverse velocity component in wind tunnels (13-16) and the optical-axis velocity component in rocket exhausts (17,18) and in an MHD generator (19).

Interferometric measurement systems offer several advantages for optical-axis velocity measurements. The Doppler shift, which is the same as for the above mentioned heterodyne system, is measurable with essentially no upper frequency limit. Also, the amount of usable scattered light is not limited by the Antenna Theorem, but instead by the etendue (light-gathering power) of the interferometer, which generally allows more of the scattered light to be used.

This paper describes a laser anemometer system using a Fabry-Perot interferometer that was designed to measure the velocity component along the optical axis for application in turbomachinery test facilities at the Lewis Research Center. A description of the optics, electronics, and the data acquistion procedures is presented. A technique is described that allows measurement of a small optical-axis velocity component, which normally is difficult because the Doppler shifted signal is masked by the non-Doppler shifted signal from surfaces located near the probe volume. Experimental results are presented for a small free-jet and for a full-annular axial-flow turbine stator cascade.

NOMENCLATURE

A	aperture area
A_s	maximum allowed aperture area of CFP
c	velocity of light
CFP	confocal Fabry-Perot interferometer
d	CFP cavity length
d_o	diameter of probe volume at $1/e^2$ intensity
D_s	diameter of central fringe of CFP
f	optical frequency

f_d	Doppler shift frequency of scattered light
f_o	frequency of laser light
f_s	frequency of scattered laser light
F	instrument finesse (small aperture)
F_e	effective finesse
FSR	free spectral range of CFP
k_o	wavenumber (magnitude of $\underset{\sim}{k}_o$), equal $2\pi/\lambda$
$\underset{\sim}{k}_o$	wavevector of incident laser beam
$\underset{\sim}{k}_s$	wavevector of scattered laser light
m	integer number
PMT	photomultiplier tube
T	transmission function of CFP
T_o	maximum transmission of CFP
U	etendue
U_s	etendue of CFP
$\underset{\sim}{v}$	velocity (vector)
v_x	velocity component along optical axis
v_T	velocity component normal to optical axis
Δf	observed standard deviation of spectral line
Δf_β	standard deviation of angular spectrum of incident beam
Δf_F	instrumental bandwidth of CFP (half-width at half-maximum)
Δf_L	standard deviation of spectral width of laser line
Δf_R	standard deviation of broadening caused by receiver aperture
Δf_T	standard deviation of broadening caused by turbulence
θ_R	angle subtended by receiver aperture at probe volume
λ	wavelength of laser
x_s	scattering angle
Ω	solid angle of field
Ω_s	maximum allowed solid angle of light incident on CFP

SCATTERING THEORY

Consider a plane wave with wave vector $\underset{\sim}{k}_o$ incident on a particle moving with velocity $\underset{\sim}{v}$ as shown in Fig. 1. Light scattered with wave vector $\underset{\sim}{k}_s$ will be Doppler shifted by an amount

$$f_d = f_s - f_o = (1/2\pi)(\underset{\sim}{k}_s - \underset{\sim}{k}_o) \cdot \underset{\sim}{v} \quad (1)$$

where f_o and f_s are the frequencies (Hz) of the incident and scattered waves, respectively. If we assume that $|\underset{\sim}{k}_s| = |\underset{\sim}{k}_o| = k_o = 2\pi/\lambda$ (a good approximation for particle velocities much less than the velocity of light), then the vector $(\underset{\sim}{k}_s - \underset{\sim}{k}_o)$ lies on the bisector of $\underset{\sim}{k}_s$ and $-\underset{\sim}{k}_o$ (i.e. along the $-x$ axis in Fig. 1). If the angle between $\underset{\sim}{k}_s$ and $\underset{\sim}{k}_o$ (the scattering angle) is x_s we can write equation (1) as

$$f_d = (2v_x/\lambda)\sin(x_s/2) \quad (2)$$

where v_x is the component of the particle's velocity along the x axis. Thus, to have the Doppler shift frequency proportional to the velocity component along the x axis, the incident and scattered light wave vectors must be symmetrically located about the x axis. For near backscatter geometry ($x_s \approx 180°$) equation (2) may be further simplified to

$$f_d = 2v_x/\lambda \quad (3)$$

A wavelength of 514.5 nm thus gives a Doppler shift of 3.887 MHz/meter/sec, which means that a Mach 1 velocity component along the system axis will have a corresponding Doppler shift of about 1.3 GHz. This rather large Doppler shift is beyond the frequency response of many commonly used photomultplier tubes, thus making heterodyne techniques difficult to apply. However, Fabry-Perot interferometers are available with free spectral ranges from about 200 MHz to many GHz.

APPARATUS

A brief discussion of the central part of this system - the confocal Fabry-Perot interferometer - is first presented. The optical system, which allows measurement of the mean velocity component along the optical axis, is then described. This is followed by a discussion of spectral broadening, which provides a basis for the measurement of turbulence intensity. Finally, the electronics and data acquistion equipment are described. In this section a technique to correct for drift in the laser frequency is given, which allows data to be accumulated over long time intervals. Also, a procedure for measuring the parameters of a spectral line with small Doppler shift is presented.

Confocal Fabry-Perot Interferometer

The confocal Fabry-Perot interferometer (CFP) is a spherical mirror optical resonator with the mirror spacing equal to the common radii of curvature of the mirrors (to within a few microns). The CFP used for this work (Fig. 2) had a mirror separation d = 37.5 mm, giving a free spectral range FSR = 2 GHz. The actual spacing is electrically adjustable over a small range by means of a piezo-electric element. Here the CFP was used as a scanning optical spectrum analyser, although it can also be used in a nonscanning mode for instantaneous velocity measurements (20).

A collimated beam of monochromatic light incident along the axis of the CFP will form a multiple beam interference pattern in the central plane of the interferometer (21). With the mirror separation at a resonance condition ($4d = m\lambda$), a bright central fringe is formed with diameter

$$D_s = 2(d^3\lambda/F)^{1/4} \quad (4)$$

where F is the instrument finesse. The specified finesse here was F = 200, so D_s = 1.2 mm.

To use the CFP as a scanning optical spectrum analyser, an aperture is placed at the CFP entrance to re-

strict transmission to the area of the central fringe. The CFP then can be considered as a bandpass filter which is scanned using the piezo-electric element. The transmittance function of the CFP for an aperture small compared to D_s is the Airy function (21)

$$T(f,d) = T_0/(1 + (2F_e/\pi)^2 \sin^2 (4\pi df/c)) \quad (5)$$

where T_0 is the maximum transmittance, c is the velocity of light, and F_e is the effective finesse defined as the ratio of the free spectral range to the observed instrumental bandwidth (full-width at half-maximum). For aperture sizes similar to or larger than the size of the central fringe the transmittance function is somewhat more complicated (21), but for the sake of simplicity we will use equation (5).

In a system such as this it is advantageous to transmit as much light as possible through the CFP to the photodetector to improve signal-to-noise ratio and to reduce data acquisition time. The measure of this light gathering power is the etendue U defined as

$$U = \Omega A \quad (6)$$

where A is the aperture area and Ω is the solid angle of the field of view subtended at the aperture.

For a CFP both Ω and A have an upper limit that can be used without an appreciable degradation in the effective finesse. These limits, here designated Ω_s and A_s, for an effective finesse $F_e = 0.7F$, are

$$A_s = \pi D_s^2/4 \quad (7)$$

$$\Omega_s = \pi\theta_s^2/4 = A_s/d^2 \quad (8)$$

The etendue of the CFP is thus

$$U_s = A_s\Omega_s = \pi^2 d\lambda/F \quad (9)$$

The aperture diameter used for this work was selected as $D_s = 1.2$ mm giving: an effective finesse $F_e = 140$; an instrumental bandwidth of 14 MHz; and an etendue $U_s = 10^{-10}$ sr-m^2.

Optical System

The optical system (Fig. 3) had both the axis of the incident beam and the axis of the receiving optics at a 3.15 degree angle to the axis of the focusing lens L1. As discussed in the Scattering Theory section, this geometry will result in a Doppler shift frequency proportional to the velocity component along the optical axis. This configuration was used instead of a direct backscatter arrangement to reduce the effective length of the probe volume to about 1 mm and thus limit the amount of extraneous light scattered into the receiving optics. In turbomachinery applications this extraneous light is particularly difficult to control because of the small passages and multiple surfaces.

Two different argon-ion lasers were used during the course of this work. Each was equipped with an etalon and produced about 0.2 Watt single-frequency output at 514.5 nm. One had a quartz rod resonator structure; its frequency stability was 60 MHz/°C. The other laser was similar, but had an aluminum resonator structure; its frequency stability was much worse, being only 14 GHz/°C. Although it is very desirable to have good frequency stability, it was found that, in a high acoustic noise environment, the laser with the aluminum resonator had less frequency jitter. Thus, in spite of its relatively poor thermal stability, this laser was used for tests in the stator cascade facility.

The laser output beam was passed through the collimator, which was adjusted to position a beam waist (diameter 100 μm at $1/e^2$ intensity) at the focal point of lens L1. The light scattered by particles in the flow passing through the probe volume is collected by lens L1 and masked by a 22-mm diameter aperture.

The scattered light, after being turned 90 degrees, is focused by lens L2 onto a pinhole aperture (diameter 100 μm). (Lenses L1 and L2 are 200 mm focal length cemented achromatic doublets corrected for spherical aberration for an object-to-image ratio of infinity.) Note that the diameter of the image of the pinhole aperture matched the $1/e^2$ intensity diameter of the incident beam waist. The dimensions of the probe volume were thus fixed by the image of the pinhole and by the angle between the incident and scattered light to be about 100-μm diameter by 1-mm depth. A 10X microscope objective L3 was placed to form an image of the pinhole (and hence the probe volume) at the CFP entrance aperture. The microscope objective and CFP were placed so that the size of the image of the pinhole aperture matched the maximum allowed aperture area of the CFP given by equation (7). (This corresponded to a magnification of 12.) Since the receiving optics aperture restricted the angular divergence of light from the probe volume to 6.3 degrees, the magnification of 12 gave an angular divergence at the CFP entrance of 0.53 degree, which is less than the maximum $\theta_s = 1.85$ degrees given by equation (8). As a result, the full light gathering capability of the CFP was not used.

The system also included an acousto-optic modulator (Bragg cell) used to generate a reference signal offset from the laser frequency by either 38.8 MHz (first order) or by 77.7 MHz (second order). This signal was used for calibration and as a stable reference for the frequency tracking circuit described in the Electronics and Data Acquisition section.

Spectral Broadening

In addition to the inherent instrumental bandwidth of the CFP given by equation (5), there are three additional factors that cause broadening of the spectral line of the light scattered by particles moving through the probe volume. One factor is fluctuations (jitter) in the laser frequency. In a controlled laboratory environment this is about ±10 MHz for time periods on the order of seconds, but will be larger for high acoustic noise or high vibration environments. This jitter in the laser frequency, of course, likewise affects the reference and non-Doppler shifted lines.

A second reason for spectral broadening is the range of scattering angles caused both by the angular spectrum of the incident beam, which can also be thought of as transit time broadening, and by the range of scattered light wave vectors. The standard deviation of the broadening due to the incident beam is (22).

$$\Delta f_B = v_T/(\pi d_0) \quad (10)$$

where v_T is the transverse velocity component and d_0 is the diameter of the probe volume. The standard deviation of the broadening due to the receiving optics aperture is

$$\Delta f_R = v_T\theta_R/(4\lambda) \quad (11)$$

where θ_R is the angle subtended by the receiver aperture at the probe volume.

The third cause of spectral broadening is fluctuations in the velocity component along the optical axis (i.e., the turbulence). This broadening effect is useful because it provides a means of using the spectral width to calculate the turbulence intensity provided that the other broadening effects are smaller.

The actual width of the observed spectral line is a convolution of the CFP instrumental bandwidth with these broadening effects. As an example, we can calculate the expected spectral width for a 200 m/sec flow velocity transverse to the optical axis with 5 percent turbulence intensity (isotropic). For the optical system shown in Fig. 3 and laser frequency jitter of 10 MHz (standard deviation), the standard deviation of the spectral line can be estimated by the root-sum-square

$$\begin{aligned}\Delta f &= (\Delta f_L^2 + \Delta f_B^2 + \Delta f_R^2 + \Delta f_F^2 + \Delta f_T^2)^{1/2}{}_{MHz} \\ &= (10^2 + 0.6^2 + 10.7^2 + 7.1^2 + 39^2)^{1/2}{}_{MHz} \\ &= 42\ MHz\end{aligned} \tag{12}$$

where one-half of the instrumental bandwidth of the CFP was used as an estimate of Δf_F since the standard deviation itself does not exist for the CFP transmittance function given by equation (5). Note that, for this example, the broadening due to the instrument only increases the spectral width due to the turbulence by about 8 percent.

Electronics and Data Acquisition

A block diagram of the electronics and data acquisition system is shown in Fig. 4. A small laboratory computer was used for data acquisition and processing; data were stored on floppy disks. A linear ramp generator, which produced a sawtooth waveform with adjustable period, amplitude, and DC offset, was used to scan the CFP over the desired frequency range. The ramp offset voltage could also be controlled with a computer generated analog signal.

Photon counting electronics were used in conjunction with the computer to record the optical spectra in histogram form. The histograms had 256 bins; each bin contained the number of photoelectron events counted during a time equal to 1/256 of the sweep duration.

The computer was programmed to operate in one of two modes. In the first mode a histogram was generated from either a single sweep of the CFP or from multiple sequential sweeps added bin-by-bin. In the second mode two histograms were generated where one histogram corresponded to data taken during even number sweeps and the other to data taken during odd number sweeps. Thus, if the flow was only seeded during alternate sweeps, one histogram was for seeded flow and the other was for unseeded flow. The difference between the two histograms (obtained by subtracting the number of counts in each bin in the unseeded histogram from the number of counts in the corresponding bin in the seeded histogram) represented the spectrum of only light scattered from the seed particles. The purpose of this procedure was to isolate the part of the spectrum due to light scattered by the seed particles from the part of the spectrum due to light scattered from surfaces near the probe volume. This mode was used to obtain the spectrum of scattered light with zero, or near-zero, Doppler shift where the spectral line of the seed particles overlapped the line from the non-Doppler shifted light.

A storage oscilloscope synchronized with the ramp generator was used to continuously monitor the analog output of the photon counter. This gave the operator a real-time picture of the spectrum being accumulated in the computer.

The computer was also used to correct for drift in the laser frequency when multiple sweeps were used. To accomplish this the peak of the Bragg cell spectral line was locked to a particular bin in the histogram by comparing the sum of the counts in two ranges consisting of an equal number of bins on each side of the reference bin. Based on this comparison, an analog output signal from the computer was used to adjust the offset voltage of the ramp generator to maintain an equal number of counts in each range. This spectrum stabilization scheme was particularly useful when the aluminum resonator laser (with its large frequency-drift rate) was used.

EXPERIMENTAL RESULTS

Two experiments were conducted to test the anemometer system. The system was first tested in a laboratory environment by measuring the flow at the exit of a small subsonic free jet. After satisfactory results were obtained in the free jet, the anemometer was installed and tested in the Lewis turbine stator test facility. This facility, because of the high acoustic noise level and because of the near zero radial flow, provided a much more demanding test of the system.

The laboratory free jet had a 9.525-mm exit diameter and was operated from the laboratory compressed air supply. The jet exit was at ambient pressure. The flow angle of the jet relative to the optical axis was set at approximately 83 degrees, which corresponded to a component along the optical axis of 12 percent of the velocity magnitude. With this particular test condition, the Doppler shifted spectral line did not overlap the unshifted spectral line. The velocity magnitude was determined by measuring the total temperature and total pressure and assuming isentropic flow through the nozzle. A silicone oil aerosol was injected upstream of the nozzle to provide seed particles.

A typical set of measurements is shown in Fig. 5, where the velocity magnitude was 243 m/sec. Fig. 5(a) shows the spectrum with no seeding - the left spectral line is the Bragg cell shifted line (shifted 38.8 MHz from the laser frequency), and the right line is the unshifted line resulting from light scattered from stationary surfaces near the probe volume. Fig. 5(b) shows the spectrum with the flow seeded and with the Bragg cell turned off - the left spectral line is the Doppler shifted line of light scattered from the seed particles and, as before, the right line is the unshifted line. (Note that the spectral lines appear broadened for the reasons discussed in the Spectral Broadening section.) Each measured spectrum (represented as a 256 bin histogram) was measured during a single 5-second sweep. The calibration factor (determined from Fig. 5(a)) was 1.01 MHz/bin, and the Doppler shift frequency (determined from Fig. 5(b)) was 114.7 MHz. Thus the velocity component along the optical axis (calculated using equation (3)) was 29.5 m/sec, and the direction was away from the anemometer. This agrees with the value calculated from the isentropic flow equations within the accuracy of the flow angle setting.

The turbulence intensity can be estimated by calculating the square root of the difference between squares of the width of the Doppler shifted line and the width of the unshifted line. For this example, the standard deviations (line widths) of the shifted and unshifted lines were 29.2 and 19.7 MHz respectively, giving a turbulence intensity of 2.3 percent. These values were determined using a 7 parameter nonlinear least squares fit of the data to a double Gaussian plus a constant (shown in the figure as a dotted line).

The second test of the anemometer was done in a 0.508 m diameter full annular cascade of 36 turbine stator vanes. The vanes, of constant profile from hub

to tip, had a height of 38.1 mm and an axial chord of 38.23 mm. In operation, atmospheric air was drawn through a bellmouth and the blading, and then was exhausted through the laboratory altitude exhaust system. The cascade was operated near the design critical velocity ratio of 0.78. A 3.2-mm thick glass cylindrical window that matched the tip radius allowed optical access to the passage. A dual-beam fringe-type laser anemometer had been previously used to map the flow in the blade to blade plane; these data, along with a description of the facility, are presented in reference (1), and in detailed form in reference (23). For this experiment the optical system was aligned to measure the radial velocity component, which was not measured with the fringe-type anemometer. It was expected that the radial velocity component would be small relative to the transverse component for this cascade.

In order to prevent excessive jitter in the laser frequency caused by the high ambient noise level (measured to be about 105 dB) it was necessary to mount the optical system in an acoustic enclosure. This enclosure was a wood box covered with two layers of an acoustical foam and lead composite. The weight of the lead was about 20 kg/m^2.

The flow was seeded with a silicone oil aerosol injected near the bellmouth entrance. A computer controlled solenoid valve in the aerosol injection line permitted use of the two-histogram data acquisition method described in the Electronics and Data Acquisition section.

A typical spectrum (taken at 50 percent axial chord, 50 percent span, and 2.3 degrees from the vane suction surface) is shown in Fig. 6. A total of 20 sweeps were used to construct the two histograms: one without seeding (Fig. 6(a)), and one with seeding (Fig. 6(b)). For this example, the time/sweep was about 1.9 seconds, giving a total data acquisition time of about 40 seconds. The reason for this relatively long acquisition time was to ensure that fluctuations in the particle arrival rate in the probe volume would not bias the measured spectrum. Also, because of the long acquisition time, multiple sweeps were necessary (rather than just two sweeps) to allow use of the spectrum stabilization procedure to compensate for drift in the laser frequency. Note that it is difficult to see the effect of the seeding in Fig. 6(b) because the Doppler shift is small compared to the line widths. Figure 6(a), which shows the unshifted spectral line on the left and the Bragg cell spectral line (shifted 77.7 MHz from the laser frequency) on the right, was used to calculate the calibration factor of 1.18 MHz/bin. This value was determined using a least squares parameter estimation procedure, where the model function was a double Gaussian plus a constant and where Poisson statistics were assumed. The fitted function is shown as a dotted line on Fig. 6(a).

The isolated Doppler shifted spectral line, obtained by subtracting the unseeded histogram from the seeded histogram, is shown in Fig. 6(c). The fit to a single Gaussian plus a constant is shown as a dotted line. Note that the deviation from the Gaussian fit is largest where the unshifted and the Bragg shifted peaks are located. Because the actual statistics are fairly complicated for this difference spectrum, the uncertainty in the amplitude was assumed constant. The difference between the Doppler shifted peak and the unshifted peak is 24.6 MHz corresponding to a radial velocity component of 6.3 m/sec toward the hub.

The square root of the difference between squares of the width of the Doppler shifted line and the width of the unshifted line gave a root-mean-square value of the radial velocity turbulence components of 4.4 m/sec, which, assuming isotropic turbulence, corresponds to a turbulence intensity of 2.4 percent.

At this location, the previous fringe system measurements (1,23) gave a velocity magnitude of 185 m/sec and a flow angle (measured from the axial direction) of 33 degrees. The standard deviation of the individual velocity measurements was 3.6 percent, which is larger than the 2.4 percent turbulence intensity calculated from the CFP measurements. One explanation for this difference is that the fringe system measurements gave only the standard deviation of the individual measurements. To infer that the turbulence intensity is equal to the standard deviation requires that the contribution of the uncertainty of the individual measurements (measurement error) be small compared to actual flow fluctuations. If this condition is not met, the standard deviation will be larger than the turbulence intensity. Also, it is unlikely that the turbulence is actually isotropic. For these reasons, the 2.4 percent turbulence intensity measured with the CFP system is believed to be consistent with the 3.6 percent standard deviation measured with the fringe system.

Additional measurements were made at various locations within the stator passage to determine how close to the end wall (hub) the radial component could be measured. It was found that the increased amount of unshifted light prevented any measurements closer than about 7 mm from the hub. This is a severe limitation. Several modifications to the system could improve its ability to measure close to surfaces. One would be to use an improved surface treatment to either absorb or specularly reflect more of the incident light. (For this work the vanes and hub were painted with an optical flat black paint to absorb the incident light.) Another improvement would be to use a multipass Fabry-Perot interferometer, which would have greatly improved contrast. Improvements could also be made in the design of the optical system to reject more of the light scattered from surfaces near the probe volume.

CONCLUSIONS

The feasibility of using a confocal Fabry-Perot interferometer for measuring the mean velocity component along the optical axis in turbomachinery operating in a high-acoustic noise environment was demonstrated. Furthermore, the system was able to measure a small mean velocity component along the optical axis, as well as turbulence intensity, by using a procedure that eliminated the part of the signal due to non-Doppler shifted light. Measurements of mean velocity taken in an annular cascade of turbine stator vanes showed reasonable agreement with expected values. In addition, the turbulence intensity calculated from the interferometer measurements was consistent with the turbulence intensity measured with a dual-beam fringe-type laser anemometer.

REFERENCES

1. Goldman, L. J., and Seasholtz, R. G., "Comparison of Laser Anemometer Measurements and Theory in an Annular Turbine Cascade with Experimental Accuracy Determined by Parameter Estimation," presented at the Symposium on Engineering Applications of Laser Velocimetry, ASME, Phoenix, Nov. 14-19, 1982.
2. Powell, J. A., Strazisar, A. J., and Seasholtz R. G., "Efficient Laser Anemometer for Intra-Rotor flow Mapping in Turbomachinery," Journal of Engineering for Power, Vol. 103, No. 2, Apr. 1981, pp. 424-429.
3. Strazisar, A. J. and Powell, J. A., "Laser Anemometer Measurements in a Transonic Axial Flow Compressor Rotor," Journal of Engineering for Power, Vol. 103, No. 2, Apr. 1981, pp. 430-437.

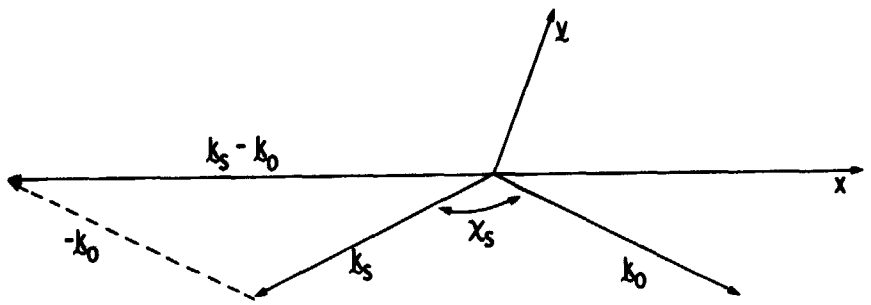

Figure 1. - Scattering geometry

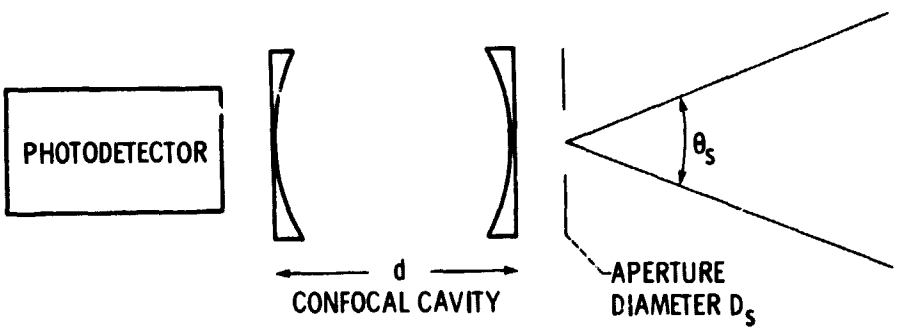

Figure 2. - Confocal Fabry Perot interferometer.

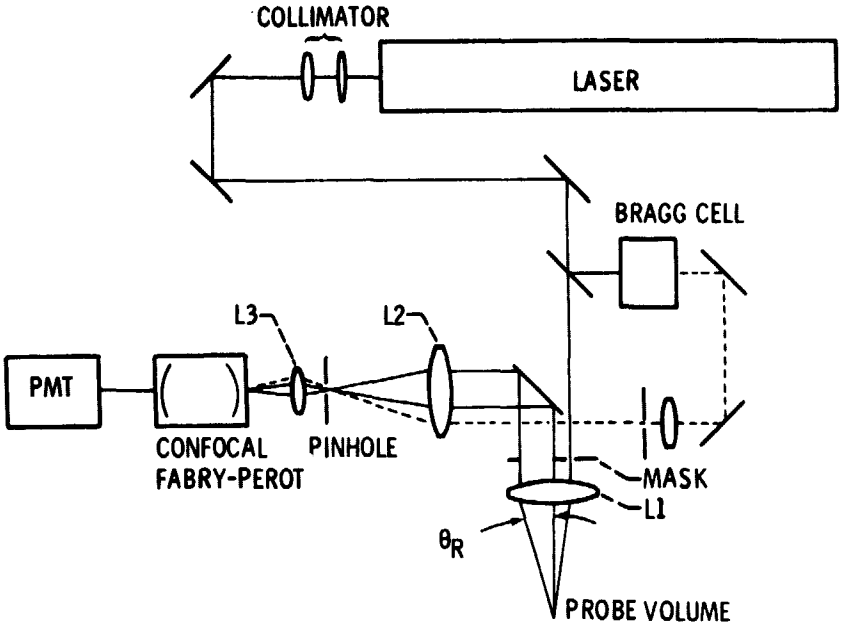

Figure 3. - Optical system.

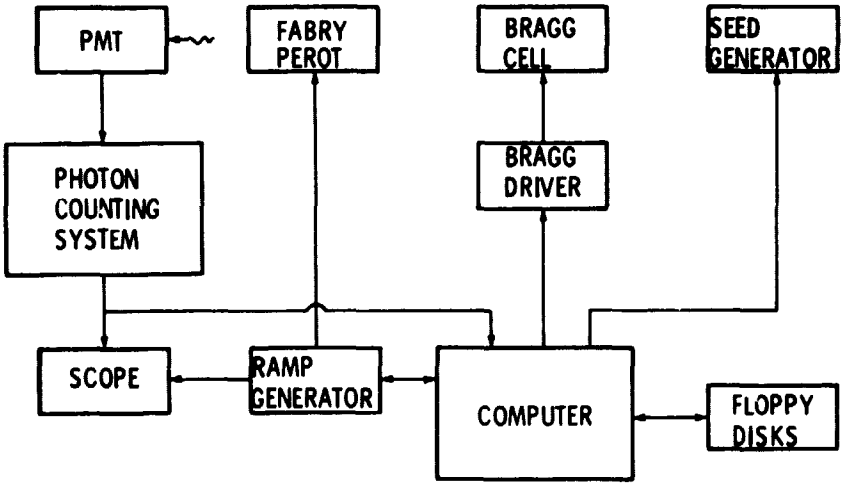

Figure 4. - Electronics and data acquisition system.

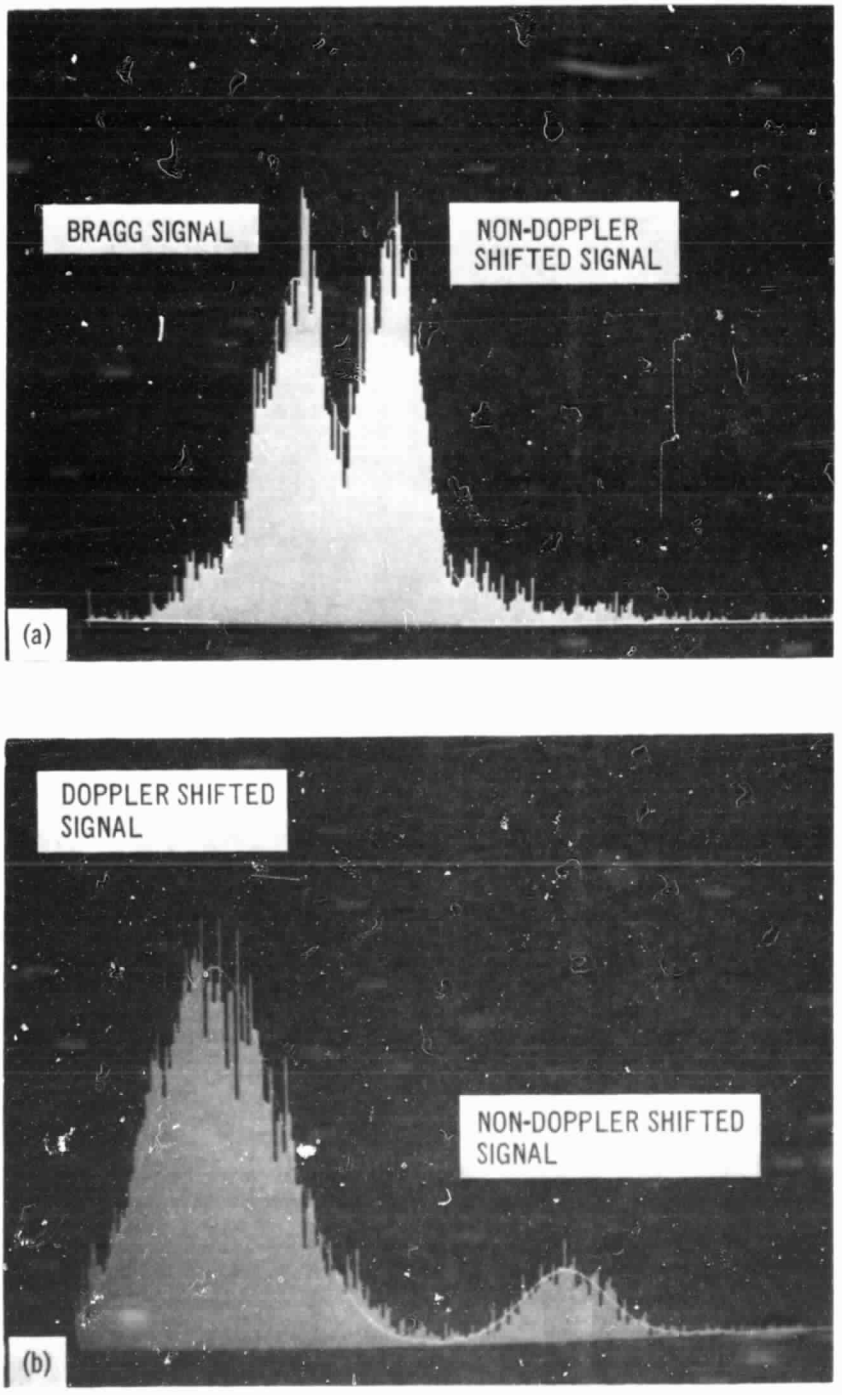

Figure 5. - Measured spectra in free jet (a) unseeded flow, Bragg cell on (b) seeded flow, Bragg cell off.

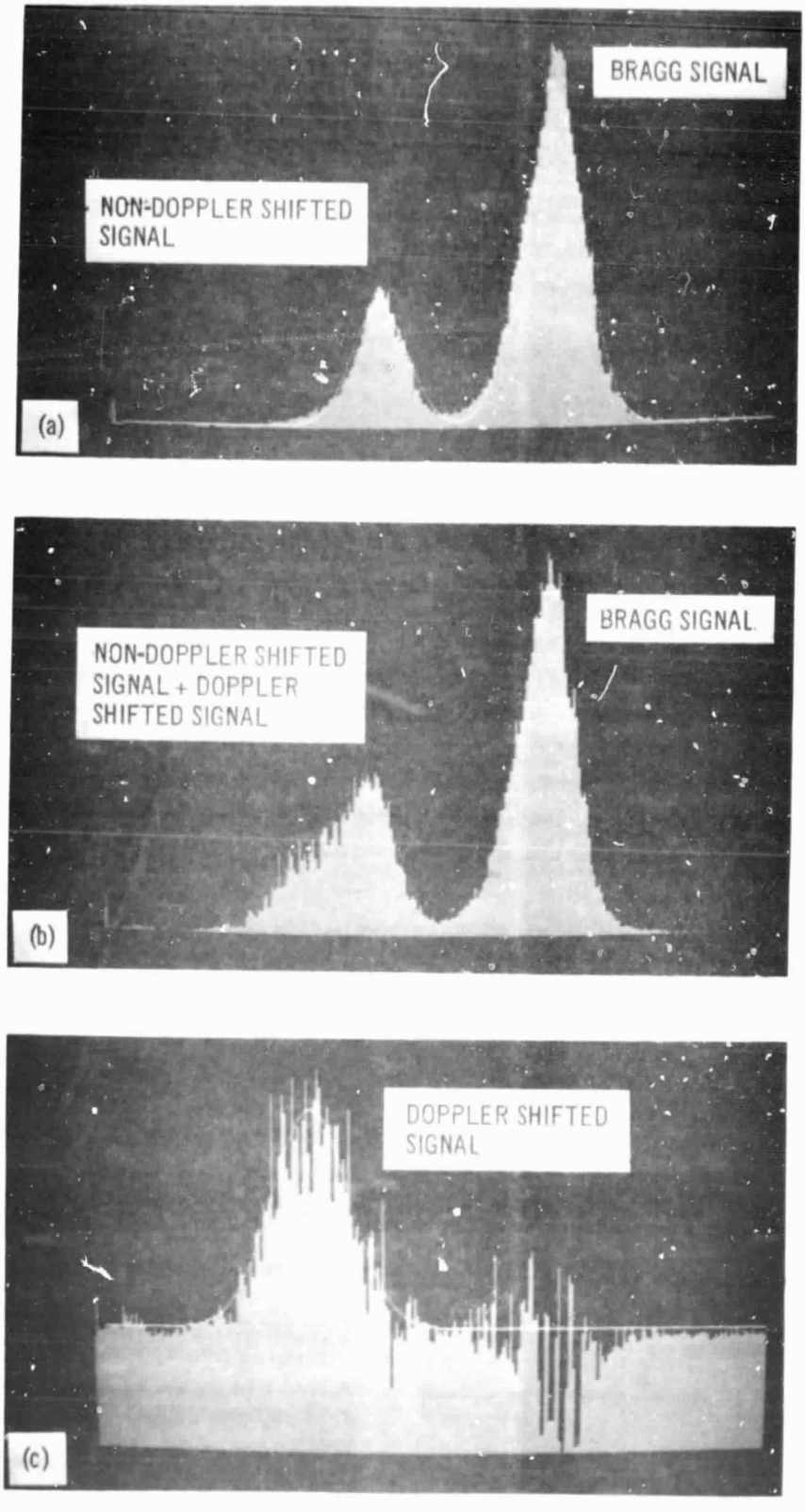

Figure 6. - Measured spectra in annular cascade (a) unseeded flow (b) seeded flow (c) difference between seeded and unseeded flow.